





Complete suppression of N₂ lasing by the nonadiabatic molecular alignment effect in femtosecond filaments

Yuxuan Zhang ^{1,*}, Renjun Yang^{2,3,*}, Zoumingyang Zhu,¹ Aurélien Houard ⁴, André Mysyrowicz,⁴ Yi Liu ^{4,5} and Pengji Ding ^{1,†}

¹*School of Nuclear Science and Technology, Lanzhou University, Lanzhou 730000, China*

²*Institute of High Energy Physics, Chinese Academy of Sciences, Beijing 100049, China*

³*Spallation Neutron Source Science Center, Dongguan 523803, China*

⁴*Laboratoire d'Optique Appliquée, ENSTA Paris, CNRS, Ecole polytechnique, Institut Polytechnique de Paris, 91162 Palaiseau, France*

⁵*Shanghai Key Laboratory of Modern Optical System, University of Shanghai for Science and Technology, Shanghai 200093, China*



(Received 13 May 2024; revised 26 July 2024; accepted 2 August 2024; published 15 August 2024)

The nonadiabatic molecular alignment effect is commonly found helpful in enhancing nonlinear processes such as high-order harmonics and strong-field ionization. In this work, an opposite phenomenon is observed, in which the nonadiabatic molecular alignment effect prepared with a linear-polarized prepulse strongly suppresses the generation of N₂ lasing induced by circularly polarized 800-nm femtosecond laser pulse in filament plasma. The presence of a weak prepulse periodically suppresses the lasing at each revival timing of the rotational wave packet of the N₂ molecule. The fine structures of the lasing suppression at different revivals exhibits distinct features. The underlying mechanism of the lasing signal suppression is attributed to sudden change of the polarization ellipticity of the pump laser pulse as it experiences ultrafast birefringence induced by the linear prepulse. Theoretical simulations by numerically solving the time-dependent Schrödinger equation with the molecular alignment effect included confirm sensitive changes of the polarization ellipticity of the pump laser at every alignment revival, which reproduces most features of the fine structures of lasing suppression and hence largely supports our interpretation.

DOI: [10.1103/PhysRevA.110.023106](https://doi.org/10.1103/PhysRevA.110.023106)

I. INTRODUCTION

“Air lasing” phenomenon, which refers to the occurrence of a laserlike coherent emission from ultrashort laser-induced filamentary plasma in ambient air, has drawn considerable attention since the early 2010s because of its rich physics in nonlinear and quantum optics on one hand, and potential applications in standoff detection on the other hand [1]. To date, such single-pass gain-swept lasing emission can be generated through three methods: (1) atomic lasing from oxygen/nitrogen species induced by deep-ultraviolet (UV) two-photon resonant pumping after predissociation of air molecules [2–5] or argon lasing using three-photon resonant pumping [6]; (2) molecular lasing from neutral nitrogen (N₂) induced by circularly polarized femtosecond laser pulse when it undergoes filamentation [7–9]; and (3) molecular lasing from singly ionized nitrogen N₂⁺ generated in femtosecond filament by linearly polarized femtosecond laser pulse [10–17]. Deep-UV pump laser suffers from strong absorption and scattering when it propagates in ambient air, hence hindering the generation and practical application of atomic lasing in atmospheric remote sensing. As for N₂⁺ lasing, although weak optical gain at 391-nm wavelength was experimentally achieved in the backward direction [18], it mainly occurs in the forward direction. Therefore, near-infrared laser-induced N₂ lasing becomes the most promising candidate for the laser source of atmospheric standoff detection in the future.

N₂ lasing occurs at 337-nm wavelength, which corresponds to the transition between the third and second excited triplet states of neutral nitrogen molecules, i.e., C³Π_u⁺(ν = 0) → B³Π_g⁺(ν' = 0) (ν and ν' represent the vibrational quantum number) [19]. After strong-field ionization, femtosecond laser pulse with circular polarization produces free electrons that distribute at higher kinetic energies but with smaller number compared to using linearly polarized pulse [20,21]. The kinetic energies of electrons are high enough to exceed the threshold of electron impact excitation of X¹Σ_g⁺ → C³Π_u⁺ via inelastic electron-molecule collision. Since electron impact excitation of X¹Σ_g⁺ → C³Π_u⁺ has a higher cross section and lower threshold of electron's kinetic energy compared to X¹Σ_g⁺ → B³Π_g⁺ [22], more N₂ molecules are excited to C³Π_u⁺ compared to B³Π_g⁺. Hence, an inversion can be established between these two states, leading to 337-nm lasing emission.

So far, generating measurable N₂ lasing emission in ambient air is still difficult due to the strong quenching effect of oxygen molecules [7]. Therefore, it is vital to seek approaches for enhancing the lasing intensity above the detection limit. One commonly used approach takes advantage of the molecular alignment effect, which nonadiabatically aligns the molecules along certain directions using a weak prepulse in advance and then irradiates the transiently aligned molecules with a strong pump pulse. In such a dynamic alignment process, the interaction between the ultrashort prepulse with respect to the rotational periods of the molecule and the molecular dipole moment gives rise to the excitation

*These authors contributed equally to this work.

†Contact author: dingpj@lzu.edu.cn

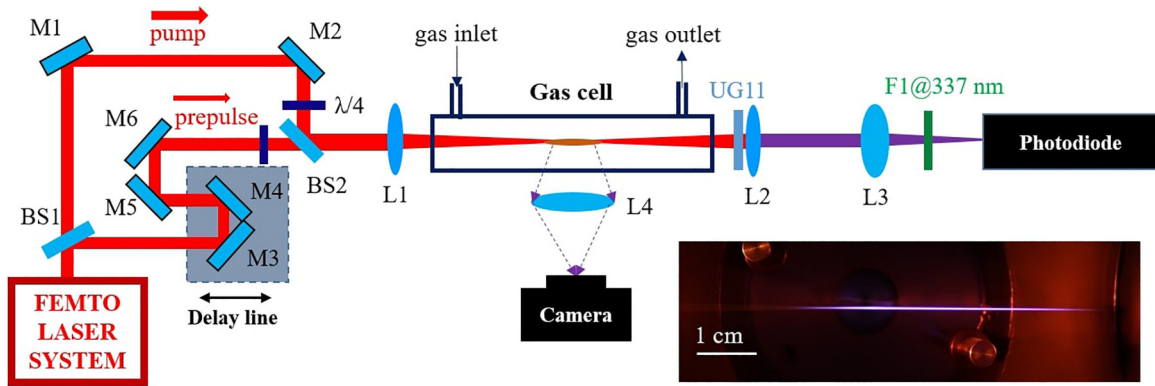


FIG. 1. Schematic of the experimental setup. BS, beamsplitter; M, high-reflectivity mirror; L, spherical lens; F, bandpass filter; and $\lambda/4$, quarter waveplate. The time delay line (TDL) is formed by a pair of mirrors fixed on an electric-controlled one-dimensional translation stage. The inset shows a luminescence image of the filament plasma created in pure nitrogen.

of a broad rotational wavepacket, whose coherence ensures alignment on turnoff of the prepulse [23,24]. Ultrashort laser-induced molecular alignment effect has been applied for manipulation or yield enhancement of high-order harmonic generation [25–27], strong-field ionization [28,29], filament-forming laser propagation [30–32], N_2^+ lasing [33–35], etc., proving to be a useful approach. For instance, Litvinyuk *et al.* determined experimentally that the ionization probability of N_2 molecules aligned parallel to the laser field is four times higher than aligned perpendicular to it [28]. More than 50% enhancement of N_2^+ lasing intensity can be achieved at half-revivals of the rotational wave packet created by the filament-forming laser pulse in nitrogen [34].

The impulsive molecular alignment effect also creates birefringence in the wake of laser filamentation. Béjot *et al.* demonstrated that the filament created with femtosecond laser pulse in atomic gases can induce substantial birefringence, which therefore acts like a wave plate that rotates the linear polarization of a delayed copropagating probe pulse [36]. The transient birefringence originates from the difference between the nonlinear refractive indices induced by the instantaneous electronic response during laser filamentation on the axes parallel and orthogonal to its polarization. Yuan *et al.* quantified such ultrafast birefringence in argon by measuring the polarization rotation of a second-harmonic-generation probe pulse propagating through the filament [37]. It was also found that the polarization of a weak probe pulse can also be modulated near the field-free revivals of preexcited rotational wavepackets created by 800-nm filamenting pulse [38]. The results suggest that the molecular alignment effect impulsively generates delayed birefringences in the wake of laser filamentation.

In this work, we investigate the influence of the nonadiabatic molecular alignment effect using an impulsive ultrashort laser on N_2 lasing in a prepulse-pump scheme. Unexpectedly, the introduction of the molecular alignment effect was found to drastically suppress the 337-nm lasing signal at both the full and fractional revivals of the rotational period of N_2 molecule.

II. EXPERIMENTAL METHOD

The experiments were carried out using a commercial chirped pulses amplification laser system (Thales Laser,

model: Alpha 100). This system delivers femtosecond laser pulses at central wavelength of 800 nm with a duration of 45 fs and a maximum pulse energy of 15 mJ at a repetition rate of 100 Hz. Figure 1 schematically illustrates the experimental setup. The output laser beam was first separated into two arms by a beamsplitter (BS1), which reflects $\sim 10\%$ of incident laser energy for the prepulse arm. The prepulse passes through a time delay line to adjust the relative delay between the pump and prepulse. The pump laser passes through a quarter waveplate, by rotating which we can control its polarization. The pump and prepulse beam are combined with another beamsplitter (BS2) and then focused with the same spherical lens (L1, $f = 1000$ mm) into a gas chamber filled with 1 bar pure nitrogen.

The circularly polarized pump laser pulse produces a bright filament plasma and generates 337-nm N_2 lasing in both the forward and backward directions. The lasing threshold is approximately 5.0 mJ. In this study, we only focus on the forward one. The forward lasing beam was collimated using a $f = 1000$ mm lens (L2) and then focused using a $f = 100$ mm lens (L3) into a calibrated photodiode. A UG11 filter, a BG39 filter, and a bandpass filter centered at 337 nm were used to block all interference light. The photodiode was connected to a lock-in amplifier and a digital acquisition system that controls the time delay line. The 337-nm lasing pulse energy was recorded in unit of mV and averaged for 100 shots for each delay time. By recording the lasing signal while scanning the relative delay between the pump and prepulse, the influence of the nonadiabatic molecular alignment effect induced by the prepulse on the lasing generation can be then investigated. The scanning step of the delay was kept at 60 fs. During the experiments, the pump pulse energy was kept around 5.8 mJ while the prepulse energy was adjustable from 100 to 700 μ J.

III. RESULTS AND DISCUSSION

Figure 2 shows the 337-nm lasing signal as a function of the relative delay between the prepulse and pump pulse. The lasing signal is normalized with respect to that without the presence of the prepulse. Positive delay ($dt > 0$) means that the prepulse arrives before the pump pulse and vice versa. The zero delay was defined as that when the strongest interference

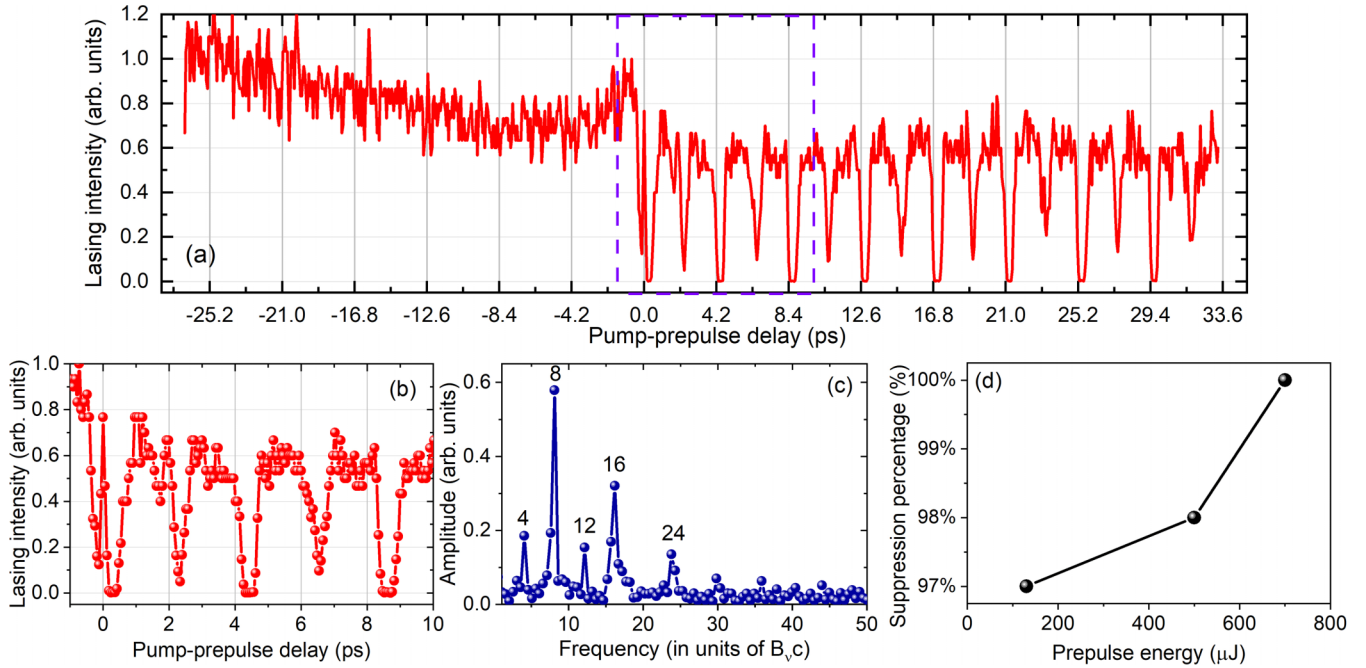


FIG. 2. (a) The 337-nm lasing signal intensity as a function of relative delay between prepulse and pump pulses. The prepulse pulse energy was approximately 700 μJ . (b) Zoomed view of the result in (a) within the first cycle of the molecular revival of the N₂ molecule. (c) Corresponding FFT result of the result in (a) for delays larger than 0, where the frequency was represented in the unit of B_vc. (d) Suppression percentage of the 337-nm lasing signal at half-revival versus the prepulse energy.

pattern occurs, which is coincident with the appearance of a narrow peak shown in Fig. 2(b).

First, let us focus on the regime of $dt < 0$. When the prepulse lags behind the pump pulse for more than ~ 25 ps, it has no noticeable influence on the lasing generation. As the prepulse approaches to the pump pulse, one can clearly see a gradual reduction of the lasing signal until $dt \sim -5$ ps. The lasing signal intensity quickly recovers within a few picoseconds as the prepulse further approaches the pump pulse. Just before the zero delay, ~ 1 ps, the lasing signal intensity reaches the local maximum, after which it sharply drops. Similar phenomena were previously observed in the pump-probe measurements of side fluorescence [39] and N₂⁺ lasing [34,35] from laser filament, but no clear explanation. Here, we interpret such behavior of 337-nm lasing signal on changing the relative delay between the pump and prepulse for $dt < 0$ as a result of destructive interference of the lagged prepulse on the gain dynamics of N₂ lasing. The prepulse interrupts the evolution of gain by either promoting the molecules in the excited C³Π_u⁺ state to higher states or/and interacting with the plasma generated by the pump pulse. Equivalently, as the prepulse approaches the pump pulse from behind, it oppositely scans the profile of the gain dynamics of N₂ lasing. Indeed, we can see that the evolution profile and temporal scale of the lasing signal versus the delay for $dt < 0$ matches well with that of the gain dynamics previously reported in Ref. [21]. At zero delay, as clearly exhibited by the narrow peak in Fig. 2(b), no enhancement but approximately 20% reduction of the lasing signal was recorded. This can be attributed to field interference between the circularly polarized pump pulse and the linearly polarized prepulse. For $dt > 0$, on the basis of a general reduction of $\sim 40\%$, the lasing signal

experiences periodic reductions at the revival times of the rotational wave packet of N₂ that has been precreated by the prepulse. The general reduction of the lasing signal lasts more than 35 ps, which can be attributed to the presence of weak plasma generated by the prepulse. This attribution is verified by the fact that a weaker prepulse alleviates the general reduction. Surprisingly, the periodic reduction occurs at every revival time, suggesting that the molecular alignment effect generally suppresses the 337-nm lasing generation.

We repeated the measurements with another two prepulse energies, e.g., 140 and 500 μJ . As shown in Fig. 2(d), a much weaker prepulse of 140 μJ can still lead to 97% suppression of the lasing signal at half-revivals compared to that without the prepulse. This result exhibits a clear difference from that of side fluorescence [39] and N₂⁺ lasing [34,35], in which the recorded signals become maximum when the molecules are aligned along the polarization direction of the prepulse and becomes minimum when they are antialigned.

Figure 3 shows detailed comparison between the results of two different prepulse energies around a series of alignment revivals including $(n + 1/4)T$, $(n + 2/4)T$, $(n + 3/4)T$ and $(n + 4/4)T$, where $n = 0, 1, 2$ represents integer numbers and T denotes the rotational period of N₂ molecule. From Fig. 3(d), the rotational period was determined as $T = 8.406$ ps. It is very close to the theoretical revival period of neutral nitrogen molecule in the ground state X¹Σ_g⁺($\nu = 0$). Given the rotational constant in the equilibrium rotational constant $B_e = 1.99824$ cm⁻¹ and the first-order ν -dependent rotational constant $\alpha_e = 0.017318$ cm⁻¹, one can get the rotational constant for X¹Σ_g⁺($\nu = 0$) state as $B_\nu = B_e - \alpha_e(\nu + 1/2) = 1.989581$ cm⁻¹ [40], which corresponds to a full revival

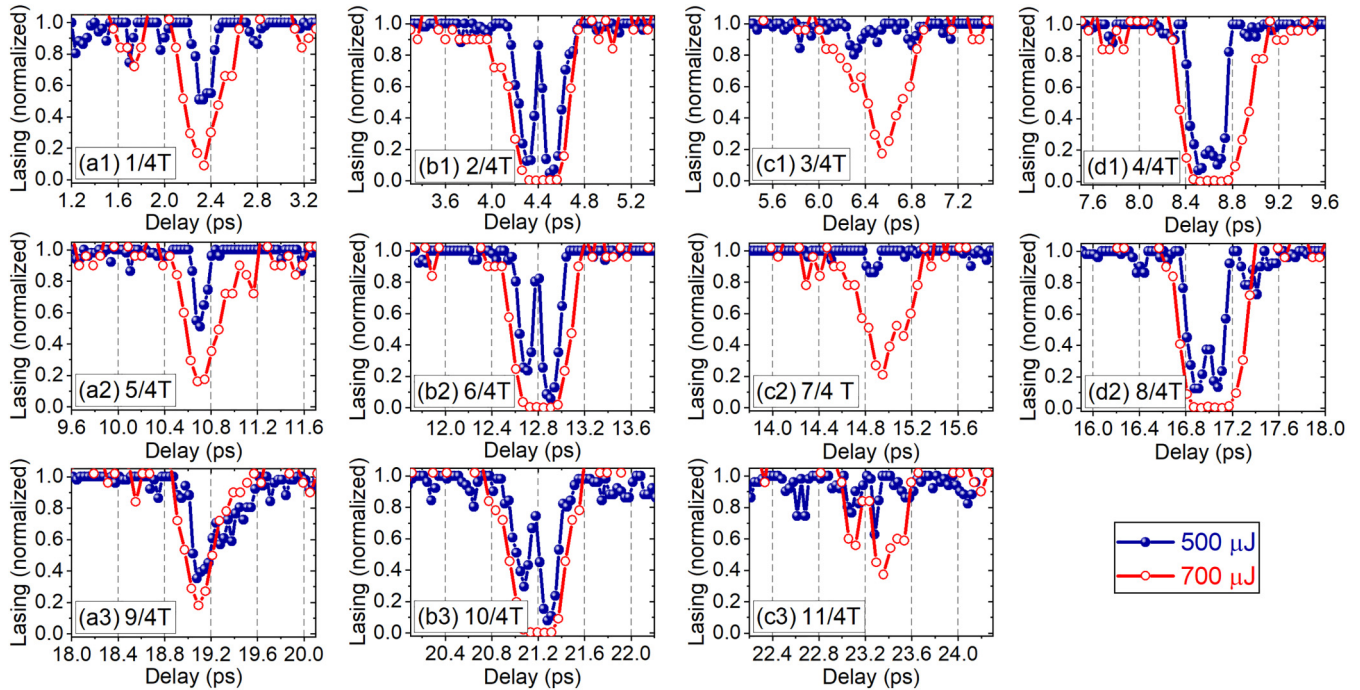


FIG. 3. Fine structures of the normalized lasing signal versus the pump-prepulse delay for two prepulse energies of 500 and 700 μJ in the vicinity of (a) $(n + 1/4)T$, (b) $(n + 2/4)T$, (c) $(n + 3/4)T$, and (d) $(n + 4/4)T$ alignment revivals.

period $T' = 1/(2B_v c) = 8.382$ ps. The slight difference between the measured revival period and the calculated one may originate from two contributions: the centrifugal distortion effect that causes slightly longer rotational periods for higher rotational levels and the potential existence of small amount of molecular nitrogen isotopes including $^{15}\text{N}_2$ and $^{14}\text{N}^{15}\text{N}$ that have smaller rotational constants.

Several observations can be drawn from Fig. 3 as follows: (1) The first one is that the extents of lasing signal suppression at $(n + 1/4)T$ and $(n + 3/4)T$ revivals are less than that at $(n + 2/4)T$ and $(n + 4/4)T$ revivals, which can be certainly attributed to their smaller alignment degrees. (2) The lasing signal suppression at $(n + 3/4)T$ revivals is apparently weaker than that at $(n + 1/4)T$ revivals for 500- μJ prepulse case, which is however not that obvious for 700 μJ . (3) Compared to the results of 700 μJ prepulse where the lasing signal was completely suppressed at $(n + 2/4)T$ and $(n + 4/4)T$, the results of 500- μJ prepulse show prominent regenerations of the lasing signal at these two alignment revivals. (4) As clearly shown in Figs. 3(b) and 3(d), the lasing signal regeneration at $(n + 2/4)T$ revival is much more prominent than that at $(n + 4/4)T$. (5) The extent of the lasing generation at $(n + 2/4)T$ revival steadily decreases from approximately 0.90 at $(1/4)T$ to 0.75 at $(10/4)T$, whereas the results at $(n + 2/4)T$ revival show increasing lasing regeneration. (6) An asymmetry of two suppression maxima around the lasing regeneration peak can be well observed in Figs. 3(b1)–3(b3). It becomes more significant as the time delay increases from $(2/4)T$ to $(10/4)T$, in which the right suppression maxima seem to remain unchanged but the left maxima steadily decrease. Such asymmetry behaves just the opposite for $(n + 4/4)T$ if one looks into the results in Figs. 3(d1) and 3(d2).

As a direct comparison, we performed another prepulse-pump experiment using a circularly polarized prepulse with an energy of ~ 730 μJ . The dependence of 337-nm lasing signal on the relative delay is shown in Fig. 4. Note that a circularly polarized femtosecond laser pulse can also produce the molecular alignment effect [41,42], but it occurs in the propagation direction and hence does not affect the pump laser in the cross-section plane. As expected, the 337-nm lasing signal is dramatically increased as two pulses spatiotemporally overlapped, an outcome of laser field interference. A weak suppression of the lasing signal is noticeable, which can be ascribed to the presence of weak plasma induced by the

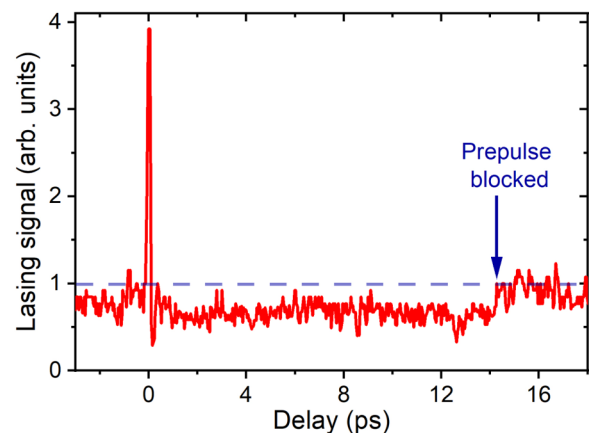


FIG. 4. The 337-nm lasing signal intensity as a function of the relative delay between the circular pump pulse and circular prepulse. The timing when the prepulse was blocked intentionally is denoted.

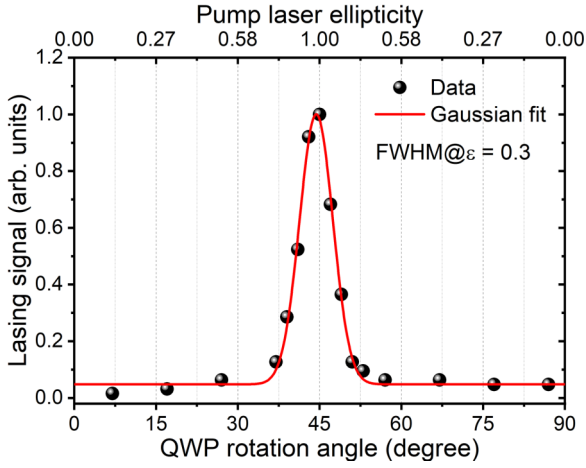


FIG. 5. Normalized 337-nm lasing signal versus the rotational angle of $1/4\text{-}\lambda$ waveplate. Gaussian fit was applied to the data to extract the FWHM of the dependence curve.

prepulse. Once the prepulse is artificially blocked, as indicated by the arrow in Fig. 4, the lasing signal intensity recovers.

The molecular alignment effect was found to be able to induce ultrafast birefringence in isotropic gas, which can change the polarization state of a delayed laser pulse [36–38,43–45]. Meanwhile, we have shown in our previous studies [7,8] that the generation of N₂ lasing in femtosecond laser filamentation only occurs when the polarization state of the pump laser pulse is very close to being circular. With the pump pulse energy of approximately 5.8 mJ, we measured the dependence of the lasing signal on the polarization ellipticity of the pump laser, as shown in Fig. 5. Same as usual, the zero and 90° of the QWP rotation angle correspond to linear polarization whereas 45° corresponds to circular polarization. One can see that the lasing signal rapidly decreases to the fluorescence level as the polarization was changed slightly away from circular. To estimate how quickly the signal decreases, a Gaussian function was applied to fit the data in Fig. 5, and the FWHM of the dependence curve is about $\Delta\epsilon = 0.3$. It indicates that the signal drops by 50% if the polarization ellipticity is changed by only 0.15 from circular.

By combining the above information, we speculate that the origin of lasing signal suppression at different revivals in Fig. 3 is that the ultrafast birefringence induced by the linearly polarized prepulse changes the polarization of the energetic pump pulse from initial circular and thus leads to significant reduction of the lasing signal. To confirm our hypothesis and better understand the experimental results, we simulated the polarization ellipticity dynamics of the pump laser pulse in the presence of a weak prepulse. We denote that the prepulse polarizes along the x axis and propagates along the z axis. The electric field of the circularly polarized pump pulse can be combined by sinusoidal oscillations $E_x(t, z)$ and $E_y(t, z)$, respectively. Their amplitudes E_{x0} and E_{y0} are equal with an phase difference $\delta_0 = \delta_{x0} - \delta_{y0} = \pi/2$. Due to the ultrafast birefringence effect, the refractive index would be modulated when the prepulse interacts with the gas medium, which leads to an external phase difference between $E_x(t, z)$ and $E_y(t, z)$ and hence change the ellipticity of the pump pulse. The

ellipticity can be described by $\tan(\delta/2)$, where δ is limited to the range of $0 \leq \delta \leq \pi/2$.

In molecular gas medium, the refractive index modulation does not only originate from the electronic Kerr effect but also from plasma formation and molecular alignment. The refractive index difference induced by the first contribution is proportional to the prepulse intensity $I_{\text{pre}}(t)$ and the nonlinear refractive index n_2 [46]:

$$\begin{aligned} \Delta n_{\text{Kerr},xy}(t) &= \Delta n_{\text{Kerr},x}(t) - \Delta n_{\text{Kerr},y}(t) \\ &= \frac{4}{3}n_2 I_{\text{pre}}(t). \end{aligned} \quad (1)$$

The generation of a filament plasma reduces the local refraction index according to the law [47]

$$\Delta n_{\text{plasma}}(t) = -\frac{\rho_e(t)}{2\rho_c}, \quad (2)$$

where ρ_e is the density of free electrons and $\rho_c = \epsilon_0 m_e \omega_0^2 / e^2$ denotes the critical plasma density above which the plasma becomes opaque. As usual, ϵ_0 , m_e , and e denote the vacuum permittivity, electron mass and charge, respectively. For a driving laser wavelength of 800 nm, $\rho_c \sim 1.7 \times 10^{21} \text{ cm}^{-3}$. In air filament, the widely reported value of ρ_e was on the order of 10^{16} cm^{-3} [48], which then results in $\Delta n_{\text{plasma}} \sim -3 \times 10^{-6}$. Besides, it was found that N₂ molecules are four times more likely to ionize when aligned parallel to the laser field than when aligned perpendicular to it [28]. Hence it is reasonable to speculate that the electron density distribution follows the same ratio, e.g., $\rho_{e,x} \approx 4\rho_{e,y}$ for x -axis polarized laser pulse. It then leads to an estimation of negative refractive index difference $\Delta n_{\text{plasma},xy} \sim -2 \times 10^{-6}$. Since the electron-ion recombination is usually of the order of nanoseconds, the filament can be considered as a stationary plasma within the probed delay range of 35 ps and hence the negative contribution of plasma formation to the refractive index difference stays constant.

The time-dependent refractive index difference caused by the nonadiabatic molecular alignment is given by [46]:

$$\begin{aligned} \Delta n_{\text{align},xy}(t) &= \Delta n_{\text{align},x}(t) - \Delta n_{\text{align},y}(t) \\ &= 3 \frac{\pi N}{n_0} \Delta\alpha \left(\langle \cos^2\theta \rangle(t) - \frac{1}{3} \right), \end{aligned} \quad (3)$$

where N and n_0 respectively represent the medium density and the refractive index on the weak field, and $\Delta\alpha = \alpha_{\parallel} - \alpha_{\perp}$ is the polarizability anisotropy defined by the difference between the polarizability components perpendicular and parallel to the molecular axis. The degree of molecular alignment is represented by $\langle \cos^2\theta \rangle(t)$, which can be obtained by following steps [49]. As a linear molecule, the rotational wave packet of N₂ after ultrashort excitation can be expanded by the rotational eigenstates $|JM\rangle$:

$$\psi(t) = \sum_J c_J(t) e^{-i\frac{E_J}{\hbar}t} |JM\rangle, \quad (4)$$

where $c_J(t)$ is the complex time-dependent coefficient, and $E_J = hcB_v J(J+1) - hcD_v J^2(J+1)^2$ is the eigenenergy of rotational state with the rotational Hamiltonian H_{rot} . Here, B_v and D_v are rigid and nonrigid rotor constants, respectively.

The evolution of $\psi(t)$ was obtained by solving the time-dependent Schrödinger equation (TDSE):

$$i\hbar \frac{\partial}{\partial t} \psi(t) = [H_{\text{rot}} - \pi \varepsilon_0 F^2(t)(\Delta\alpha \cos^2\theta + \alpha_{\perp})] \psi(t), \quad (5)$$

where ε_0 and $F(t)$ are the vacuum permittivity and the electric field of the laser pulse. After obtaining the time-dependent coefficient $c_J(t)$ by Eq. (5), the alignment degree of an initial eigenstate $|JM\rangle$ can be calculated:

$$\langle \cos^2\theta \rangle_{JM}(t) = \langle \psi_{JM}(t) | \cos^2\theta | \psi_{JM}(t) \rangle, \quad (6)$$

where the initial state of $\psi_{JM}(t)$ is $|JM\rangle$. By considering the Boltzmann distribution of the initial molecular states, the alignment degree of the molecules can be calculated:

$$\langle \langle \cos^2\theta \rangle \rangle(t) = \sum_J W_J \sum_{M=-J}^J \langle \cos^2\theta \rangle_{JM}(t), \quad (7)$$

where W_J is the Boltzmann weight factor. After calculating the refractive index difference induced by the prepulse, the phase difference of the pump pulse between the x axis and the y axis can be obtained by:

$$\delta(t) = \frac{2\pi}{\lambda} [\Delta n_{\text{Kerr},xy}(t) + \Delta n_{\text{plasma},xy} + \Delta n_{\text{align},xy}(t)]L + \delta_0, \quad (8)$$

where λ is the center wavelength of the pump pulse.

By assuming that the prepulse mainly interacts with the nitrogen gas in a cylindrical filamentary column, we numerically simulated the modulation of the polarization ellipticity of the pump pulse when it propagates through the birefringent medium prepared by the prepulse. Considering a practical filament diameter of approximately 200 μm [50], the average laser intensity inside the filament created by the 700- μJ prepulse can be estimated as $5 \times 10^{13} \text{ W/cm}^2$. We performed simulations for two different prepulse intensities, $5 \times 10^{13} \text{ W/cm}^2$ and $3 \times 10^{13} \text{ W/cm}^2$. We set $\Delta n_{\text{plasma},xy} = -2 \times 10^{-6}$ for the former intensity, and -2×10^{-7} for the latter one considering the multiphoton ionization scaling law. The filament length was set to $L = 1 \text{ cm}$. Figure 6 shows simulated evolution of the molecular alignment degree $\langle \langle \cos^2\theta \rangle \rangle$, the total refractive index change Δn and the polarization ellipticity of the pump laser as the relative delay between the circular pump and linear prepulse varies within the first revival period. Most importantly, one can observe that the polarization ellipticity of the pump laser will be significantly modulated in the wake of the linear prepulse around the vicinity of integral multiples of the quarter revival, in which stronger alignment effect results in larger ellipticity shift from initial circular polarization. If using an intenser prepulse, then the ellipticity modulation of the pump pulse becomes more significant. Given the generation of the 337-nm lasing is sensitive to the ellipticity of the pump pulse, a sudden polarization change of the pump laser pulse leads to the disappearance of the lasing signal when the ellipticity is lower than the threshold of approximately 0.7. Around the zero time delay, all three mechanisms including the instantaneous electronic Kerr effect, plasma formation and adiabatic molecular alignment effect contribute to the fast drop of the pump laser ellipticity from $\epsilon = 1$.

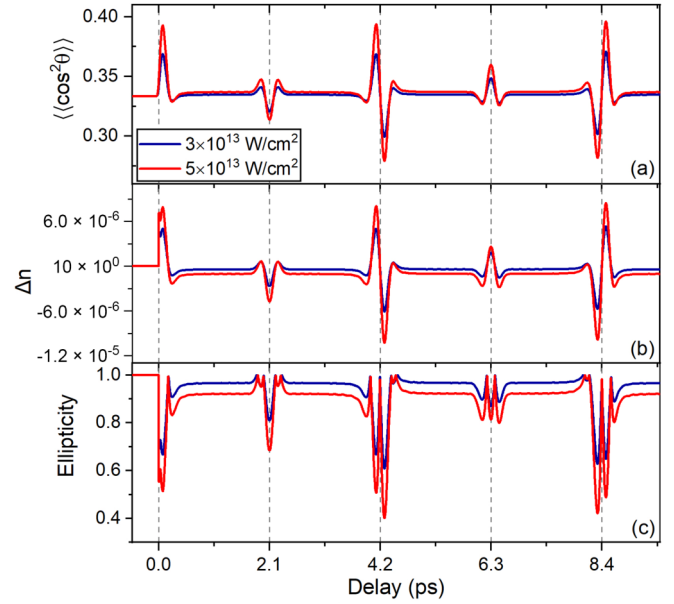


FIG. 6. Simulated results of (a) the molecular alignment degree $\langle \langle \cos^2\theta \rangle \rangle$, (b) the refractive index change and (c) the polarization ellipticity of the pump laser pulse as a function of the relative time delay between the circular pump laser pulse and the linear prepulse.

After the passage of the prepulse, the long-lived presence of plasma introduces a constant shift to the pump laser ellipticity, whereas the nonadiabatic alignment effect leads to its periodic modulations. Note that the refractive index change due to molecular alignment effect is on the same order of magnitude with that owing to plasma formation, which manifests itself as the baseline in Fig. 6(b).

The simulated fine structure of the laser ellipticity evolution is shown in Fig. 7, which reproduces most of the features observed in the experiments. First, the ellipticity shift at $(n + 1/4)T$ exhibits more prominent than $(n + 3/4)T$, which qualitatively agrees with the experimental feature with 500- μJ prepulse shown in Fig. 3. Second, the ellipticity shift occurs at both aligned and antialigned moments, and the shift at the latter moment is obviously larger than that at the former one. If we compare the simulated results at $(n + 2/4)T$ and $(n + 4/4)T$ in Figs. 7(b) and 7(d), then they show opposite characteristics that qualitatively agree with the experimental observations in Figs. 3(b) and 3(c). It should be noted that above two features can only be achieved after introducing the negative refractive index change from anisotropic plasma formation.

As the time delay increases, as shown in Figs. 7(b1)–7(b3), the ellipticity shifts at the aligned moments around $(n + 2/4)T$ revivals becomes smaller while the shifts at the antialign moments increases, making the difference of two peaks more significant. The simulated results around $(n + 4/4)T$ revivals show exactly same trend. This feature is also in good agreement with the experimental observations in Figs. 3(b) and 3(c). The underlying reason of this time-dependent asymmetry between the ellipticity shifts at the aligned and antialigned moments relates to the detuning of the rotational wave packet induced by the centrifugal distortion effect that considers the nitrogen molecule as a nonrigid rotor.

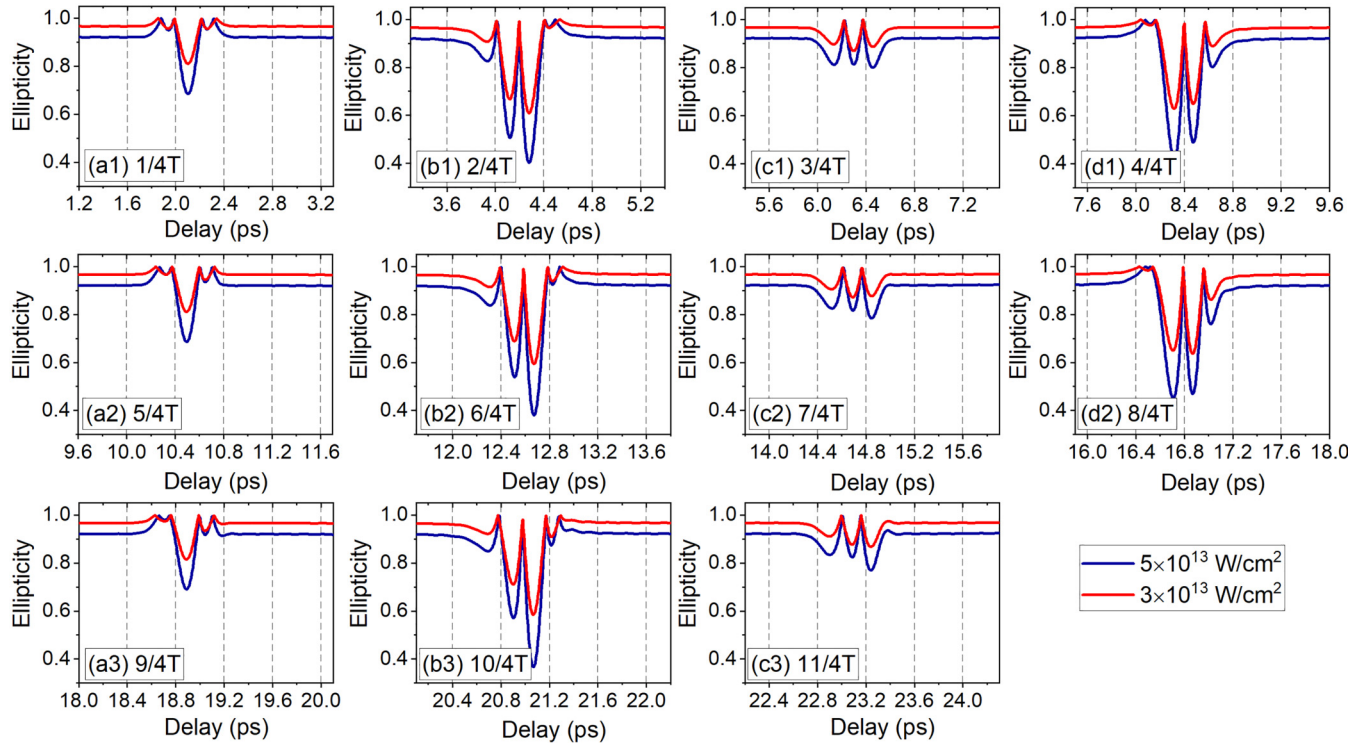


FIG. 7. Simulated polarization ellipticity of the driving laser pulse as a function of the relative time delay between the circular pump laser pulse and the linear prepulse in the revival vicinity of (a) $(n + 1/4)T$, (b) $(n + 2/4)T$, (c) $(n + 3/4)T$, (d) $(n + 4/4)T$ for two prepulse intensities: $3 \times 10^{13} \text{ W/cm}^2$ and $5 \times 10^{13} \text{ W/cm}^2$.

Higher rotational levels have slightly longer rotational periods and hence the temporal difference between these periods becomes increasingly larger with the time. That will lead to an increasingly larger asymmetry.

It should be noted that two features observed in the experimental results in Fig. 3, e.g., the damping recovery of the lasing signal with the time at $(n + 2/4)T$ revival and a much stronger lasing recovery at $(n + 2/4)T$ revival compared to $(n + 4/4)T$, were not reproduced in the simulations. The first feature could originate from the collisional decay of rotational coherence, which was not included in the simulations. As a result of growing dispersion in the rotational wave packet with the time, the molecular alignment degrades and hence the induced birefringence effect for a delayed pump laser becomes weaker as the delay increases. The second feature certainly relates to the ultrafast transition direction of the rotationally excited molecules from being aligned to antialigned or vice versa. The experimental results suggest that the lasing recovery favors the transition direction from aligned to antialigned rather than the opposite. The failure to reproduce this feature in the simulation suggests that the current theoretical model is not yet complete, which then requires deeper investigations.

IV. CONCLUSION

To conclude, we experimentally found that the molecular alignment effect plays a detrimental influence on 337-nm lasing generation of N₂ molecules in laser filamentation that

is created by circularly polarized near-IR femtosecond laser pulse. The molecular alignment prepared by a linearly polarized near-IR prepulse, which is much weaker and temporally ahead of the pump laser pulse, periodically suppresses the lasing generation at each revival of rotational wave packets. A prepulse with only 140 μJ energy can suppress the lasing signal intensity by 97%. It was observed that stronger alignment degree leads to more significant lasing suppression. The fine evolution structures of the lasing signal near the revivals were analyzed, which show distinct features between the structures around $(n + 1/4)T$ and $(n + 3/4)T$ as well as the structures around $(n + 2/4)T$ and $(n + 4/4)T$. The lasing suppression at $(n + 1/4)T$ revival appears stronger than that at $(n + 3/4)T$ one. A growing asymmetry between two suppression peaks at $(n + 2/4)T$ revival with increasing time delays between the pump pulse and prepulse was observed whereas an opposite evolution was noticed at $(n + 4/4)T$ revival.

The underlying mechanism of the lasing suppression by the molecular alignment effect was hypothetically attributed to the sudden change of the polarization ellipticity of the pump laser pulse when it experiences ultrafast birefringence induced by the prepulse. Theoretical simulations by numerically solving the TDSE reveal sensitive changes in the polarization ellipticity of the pump laser pulse at every alignment revival. The simulated behavior of the pump laser ellipticity captured most of the observed features in the fine structure of lasing suppression, such as stronger alignment degree inducing a larger ellipticity drop and more significant asymmetry between two suppression peaks at $(n + 2/4)T$ with

the increasing time delay. However, the simulation fails to reproduce two experimental observations, e.g., the damping recovery of the lasing signal at $(n + 2/4)T$ revival and a much stronger lasing recovery at $(n + 2/4)T$ revival compared to $(n + 4/4)T$. Possible reasons were briefly discussed. In the end, it becomes clear that current theoretical model requires further completeness to fully reproduce the experimental observations.

ACKNOWLEDGMENTS

This research work is supported by the National Science Foundation for Young Scientists of China (Grants No. 12004147, No. 12305166, and No. 12034013), the open project of Shanghai Institute of Optics and Fine Mechanics (SIOM, Chinese Academy of Sciences), and Guangdong Basic and Applied Basic Research Foundation (2022A1515140179).

-
- [1] P. Polynkin and Y. Cheng (eds.), *Air Lasing* (Springer International, New York, 2018), p. 208.
- [2] A. Dogariu, J. B. Michael, M. O. Scully, and R. B. Miles, High-gain backward lasing in air, *Science* **331**, 442 (2011).
- [3] A. Laurain, M. Scheller, and P. Polynkin, Low-threshold bidirectional air lasing, *Phys. Rev. Lett.* **113**, 253901 (2014).
- [4] P. Ding, M. Ruchkina, Y. Liu, M. Alden, and J. Bood, Femtosecond two-photon-excited backward lasing of atomic hydrogen in a flame, *Opt. Lett.* **43**, 1183 (2018).
- [5] P. Ding, M. Ruchkina, Y. Liu, M. Alden, and J. Bood, Gain mechanism of femtosecond two-photon-excited lasing effect in atomic hydrogen, *Opt. Lett.* **44**, 2374 (2019).
- [6] A. Dogariu and R. B. Miles, Three-photon femtosecond pumped backwards lasing in argon, *Opt. Express* **24**, A544 (2016).
- [7] S. Mitryukovskiy, Y. Liu, P. Ding, A. Houard, and A. Mysyrowicz, Backward stimulated radiation from filaments in nitrogen gas and air pumped by circularly polarized 800 nm femtosecond laser pulses, *Opt. Express* **22**, 12750 (2014).
- [8] P. Ding, S. Mitryukovskiy, A. Houard, E. Oliva, A. Couairon, A. Mysyrowicz, and Y. Liu, Backward lasing of air plasma pumped by circularly polarized femtosecond pulses for the saKe of remote sensing (BLACK), *Opt. Express* **22**, 29964 (2014).
- [9] J. Yao, H. Xie, B. Zeng, W. Chu, G. Li, J. Ni, H. Zhang, C. Jing, C. Zhang, H. Xu, Y. Cheng, and Z. Xu, Gain dynamics of a free-space nitrogen laser pumped by circularly polarized femtosecond laser pulses, *Opt. Express* **22**, 19005 (2014).
- [10] J. Yao, B. Zeng, H. Xu, G. Li, W. Chu, J. Ni, H. Zhang, S. L. Chin, Y. Cheng, and Z. Xu, High-brightness switchable multiwavelength remote laser in air, *Phys. Rev. A* **84**, 051802(R) (2011).
- [11] H. Xu, E. Lötstedt, A. Iwasaki, and K. Yamanouchi, Sub-10-fs population inversion in N_2^+ in air lasing through multiple state coupling, *Nat. Commun.* **6**, 8347 (2015).
- [12] Y. Liu, P. Ding, G. Lambert, A. Houard, V. Tikhonchuk, and A. Mysyrowicz, Recollision-induced superradiance of ionized nitrogen molecules, *Phys. Rev. Lett.* **115**, 133203 (2015).
- [13] J. Yao, S. Jiang, W. Chu, B. Zeng, C. Wu, R. Lu, Z. Li, H. Xie, G. Li, C. Yu, Z. Wang, H. Jiang, Q. Gong, and Y. Cheng, Population redistribution among multiple electronic states of molecular nitrogen ions in strong laser fields, *Phys. Rev. Lett.* **116**, 143007 (2016).
- [14] Y. Liu, P. Ding, N. Ibrakovic, S. Bengtsson, S. Chen, R. Danylo, E. R. Simpson, E. W. Larsen, X. Zhang, Z. Fan, A. Houard, J. Mauritsson, A. L'Huillier, C. L. Arnold, S. Zhuang, V. Tikhonchuk, and A. Mysyrowicz, Unexpected sensitivity of nitrogen ions superradiant emission on pump laser wavelength and duration, *Phys. Rev. Lett.* **119**, 203205 (2017).
- [15] H. Li, M. Hou, H. Zang, Y. Fu, E. Lötstedt, T. Ando, A. Iwasaki, K. Yamanouchi, and H. Xu, Significant enhancement of N_2^+ lasing by polarization-modulated ultrashort laser pulses, *Phys. Rev. Lett.* **122**, 013202 (2019).
- [16] T. Ando, E. Lötstedt, A. Iwasaki, H. Li, Y. Fu, S. Wang, H. Xu, and K. Yamanouchi, Rotational, vibrational, and electronic modulations in N_2^+ lasing at 391 nm: Evidence of coherent $B^2\Sigma_u^+ - X^2\Sigma_g^+ - A^2\Pi_u$ coupling, *Phys. Rev. Lett.* **123**, 203201 (2019).
- [17] A. Mysyrowicz, R. Danylo, A. Houard, V. Tikhonchuk, X. Zhang, Z. Fan, Q. Liang, S. Zhuang, L. Yuan, and Y. Liu, Lasing without population inversion in N_2^+ , *APL Photon.* **4**, 110807 (2019).
- [18] X. Zhang, R. Danylo, Z. Fan, P. Ding, C. Kou, Q. Liang, A. Houard, V. Tikhonchuk, A. Mysyrowicz, and Y. Liu, Backward lasing of singly ionized nitrogen ions pumped by femtosecond laser pulses, *Appl. Phys. B* **126**, 53 (2020).
- [19] Q. Luo, W. Liu, and S. Chin, Lasing action in air induced by ultra-fast laser filamentation, *Appl. Phys. B* **76**, 337 (2003).
- [20] S. Mitryukovskiy, Y. Liu, P. Ding, A. Houard, A. Couairon, and A. Mysyrowicz, Plasma luminescence from femtosecond filaments in air: Evidence for impact excitation with circularly polarized light pulses, *Phys. Rev. Lett.* **114**, 063003 (2015).
- [21] P. Ding, E. Oliva, A. Houard, A. Mysyrowicz, and Y. Liu, Lasing dynamics of neutral nitrogen molecules in femtosecond filaments, *Phys. Rev. A* **94**, 043824 (2016).
- [22] Y. Itikawa, Cross sections for electron collisions with nitrogen molecules, *J. Phys. Chem. Ref. Data* **35**, 31 (2006).
- [23] T. Seideman and E. Hamilton, *Nonadiabatic Alignment by Intense Pulses. Concepts, Theory, and Directions* (Academic Press, San Diego, CA, 2005), pp. 289–329.
- [24] H. Stapelfeldt and T. Seideman, *Colloquium: Aligning molecules with strong laser pulses*, *Rev. Mod. Phys.* **75**, 543 (2003).
- [25] R. Velotta, N. Hay, M. B. Mason, M. Castillejo, and J. P. Marangos, High-order harmonic generation in aligned molecules, *Phys. Rev. Lett.* **87**, 183901 (2001).
- [26] J. Itatani, D. Zeidler, J. Levesque, M. Spanner, D. M. Villeneuve, and P. B. Corkum, Controlling high harmonic generation with molecular wave packets, *Phys. Rev. Lett.* **94**, 123902 (2005).
- [27] K. Miyazaki, M. Kaku, G. Miyaji, A. Abdurrouf, and F. H. M. Faisal, Field-free alignment of molecules observed with high-order harmonic generation, *Phys. Rev. Lett.* **95**, 243903 (2005).
- [28] I. V. Litvinyuk, K. F. Lee, P. W. Dooley, D. M. Rayner, D. M. Villeneuve, and P. B. Corkum, Alignment-dependent strong field ionization of molecules, *Phys. Rev. Lett.* **90**, 233003 (2003).

- [29] S. J. Weber, M. Oppermann, and J. P. Marangos, Role of rotational wave packets in strong field experiments, *Phys. Rev. Lett.* **111**, 263601 (2013).
- [30] F. Calegari, C. Vozzi, S. Gasilov, E. Benedetti, G. Sansone, M. Nisoli, S. De Silvestri, and S. Stagira, Rotational Raman effects in the wake of optical filamentation, *Phys. Rev. Lett.* **100**, 123006 (2008).
- [31] S. Varma, Y.-H. Chen, and H. M. Milchberg, Trapping and destruction of long-range high-intensity optical filaments by molecular quantum wakes in air, *Phys. Rev. Lett.* **101**, 205001 (2008).
- [32] B. Shim, S. E. Schrauth, A. L. Gaeta, M. Klein, and G. Fibich, Loss of phase of collapsing beams, *Phys. Rev. Lett.* **108**, 043902 (2012).
- [33] M. Richter, M. Lytova, F. Morales, S. Haessler, O. Smirnova, M. Spanner, and M. Ivanov, Rotational quantum beat lasing without inversion, *Optica* **7**, 586 (2020).
- [34] H. Xu, E. Lötstedt, T. Ando, A. Iwasaki, and K. Yamanouchi, Alignment-dependent population inversion in N₂⁺ in intense few-cycle laser fields, *Phys. Rev. A* **96**, 041401(R) (2017).
- [35] R. Danylo, G. Lambert, Y. Liu, V. Tikhonchuk, A. Houard, and A. Mysyrowicz, Quantum erasing of laser emission in N₂⁺, *Opt. Lett.* **45**, 4670 (2020).
- [36] P. Béjot, Y. Petit, L. Bonacina, J. Kasparian, M. Moret, and J.-P. Wolf, Ultrafast gaseous “half-wave plate,” *Opt. Express* **16**, 7564 (2008).
- [37] S. Yuan, T.-J. Wang, O. Kosareva, N. Panov, V. Makarov, H. Zeng, and S. L. Chin, Measurement of birefringence inside a filament, *Phys. Rev. A* **84**, 013838 (2011).
- [38] S. Yuan, T.-J. Wang, H. Pan, L. Zheng, S. L. Chin, and H. Zeng, Pulse polarization evolution and control in the wake of molecular alignment inside a filament, *Opt. Express* **23**, 5582 (2015).
- [39] A. Azarm, S. Ramakrishna, A. Talebpour, S. Hosseini, Y. Teranishi, H. L. Xu, Y. Kamali, J. Bernhardt, S. H. Lin, T. Seideman, and S. L. Chin, Population trapping and rotational revival of N₂ molecules during filamentation of a femtosecond laser pulse in air, *J. Phys. B: At., Mol. Opt. Phys.* **43**, 235602 (2010).
- [40] J. Bendtsen, The rotational and rotation-vibrational Raman spectra of ¹⁴N₂, ¹⁴N¹⁵N and ¹⁵N₂, *J. Raman Spectrosc.* **2**, 133 (1974).
- [41] C. T. L. Smeenk and P. B. Corkum, Molecular alignment using circularly polarized laser pulses, *J. Phys. B: At. Mol. Opt. Phys.* **46**, 201001 (2013).
- [42] N. Kaya, J. Strohaber, A. A. Kolomenskii, and H. A. Schuessler, Effect of circularly polarized femtosecond laser pulses on alignment dynamics of linear molecules observed by strong-field photoelectron yields, *Eur. Phys. J. D* **70**, 224 (2016).
- [43] C. Marceau, Y. Chen, F. Théberge, M. Châteauneuf, J. Dubois, and S. L. Chin, Ultrafast birefringence induced by a femtosecond laser filament in gases, *Opt. Lett.* **34**, 1417 (2009).
- [44] V. Renard, M. Renard, S. Guérin, Y. T. Pashayan, B. Lavorel, O. Faucher, and H. R. Jauslin, Postpulse molecular alignment measured by a weak field polarization technique, *Phys. Rev. Lett.* **90**, 153601 (2003).
- [45] O. Kosareva, N. Panov, V. Makarov, I. Perezhogin, C. Marceau, Y. Chen, S. Yuan, T. Wang, H. Zeng, A. Savel’ev, and S. L. Chin, Polarization rotation due to femtosecond filamentation in an atomic gas, *Opt. Lett.* **35**, 2904 (2010).
- [46] C. Marceau, S. Ramakrishna, S. Génier, T.-J. Wang, Y. Chen, F. Théberge, M. Châteauneuf, J. Dubois, T. Seideman, and S. L. Chin, Femtosecond filament induced birefringence in argon and in air: Ultrafast refractive index change, *Opt. Commun.* **283**, 2732 (2010).
- [47] M. D. Feit and J. A. Fleck, Jr., Effect of refraction on spot-size dependence of laser-induced breakdown, *Appl. Phys. Lett.* **24**, 169 (1974).
- [48] A. Couairon and A. Mysyrowicz, Femtosecond filamentation in transparent media, *Phys. Rep.* **441**, 47 (2007).
- [49] H. Hasegawa and Y. Ohshima, Nonadiabatic molecular alignment and orientation, in *Progress in Ultrafast Intense Laser Science XII*, edited by K. Yamanouchi, L. Roso, R. Li, D. Mathur, and D. Normand (Springer International, Cham, 2015), pp. 45–64.
- [50] S. I. Mitryukovskiy, Y. Liu, A. Houard, and A. Mysyrowicz, Re-evaluation of the peak intensity inside a femtosecond laser filament in air, *J. Phys. B: At. Mol. Opt. Phys.* **48**, 094003 (2015).